ISSN 2071-1859 (Print), ISSN 2521-6635 (Online)
UDC 624.012.45:623.1 https://doi.org/10.33271/crpnmu/86.230

© N. Zuievska[1], V. Berezdetskyi[1], D. Darmostuk[1], R. Semchuk[1], O. Khalymendyk[2]
[1]National Technical University of Ukraine "Igor Sikorsky Kyiv Polytechnic Institute", Kyiv, Ukraine
[2]Dnipro University of Technology, Dnipro, Ukraine

NUMERICAL SIMULATION OF COMBINED PENETRATION AND EXPLOSION EFFECTS ON THE TWO-LAYER ROOF OF SHALLOW-BURIED CRITICAL INFRASTRUCTURE PROTECTIVE STRUCTURES

Н.В. Зуєвська[1], https://orcid.org/0000-0002-1716-1447
В.Ю.Березdецький[1], https://orcid.org/0009-0004-1007-975X
Д.Г. Дармостук[1], https://orcid.org/0009-0002-3714-9821
Р.І. Семчук[1], https://orcid.org/0009-0007-1336-6246
О.В. Халимендик[2] https://orcid.org/0000-0002-1311-1135
[1]Національний технічний університет України «Київський політехнічний інститут імені Ігоря Сікорського», Київ, Україна
[2]Національний технічний університет «Дніпровська політехніка», Дніпро, Україна

ЧИСЕЛЬНЕ МОДЕЛЮВАННЯ КОМБІНОВАНОЇ ДІЇ ПРОНИКНЕННЯ ТА ВИБУХУ НА ДВОШАРОВЕ ПОКРИТТЯ МАЛОЗАГЛИБЛЕНИХ ЗАХИСНИХ СПОРУД КРИТИЧНОЇ ІНФРАСТРУКТУРИ

Purpose. Substantiation of a two-layer roof design for shallow-buried protective structures of critical infrastructure and quantitative assessment of its stress–strain state under the combined impact-and-blast action of a munition in comparison with the action of a surface-laid (contact) charge.

The methods. Numerical simulation in the coupled Euler–Lagrange formulation of ANSYS Explicit Dynamics. Concrete is described by the RHT strength model with the P–α equation of state, detonation products by the JWL equation of state, and air by the ideal gas model. The roof consists of an upper sacrificial slab 600 mm thick, an air gap, and a load-bearing deck of adjacent concrete beams. The munition contains 100 kg of high explosive in an aluminum casing, with an approach velocity of 139 m/s and a detonation delay of 14.1 ms. A parametric series of simulations was performed for charge masses of 100–500 kg TNT equivalent.

Findings. The combined impact-and-blast loading is shown to produce peak tensile stresses of 25.5 MPa in the lower part of the structure, compared with 2.78 MPa for a contact charge of the same mass. For the contact charge, a power-law dependence of peak stress on charge mass, $\sigma_1^p \approx 0.20W^{0.51}$, was obtained, consistent with the energy similarity laws of explosion; the peak stress in the impact-and-blast scenario is practically independent of charge mass (26.5 ± 1.0 MPa) and is governed by the impact velocity and the acoustic impedances of the materials. Damage to the deck is localized within one to three beams beneath the impact zone.

The originality. For the first time, the stress time histories of a spaced two-layer roof have been compared for a contact charge and for the coupled "impact + detonation" scenario; an engineering relationship for peak tensile stresses is proposed based on the transmission coefficient of the impact contact stress.

Practical implementation. The simplified contact-charge design scheme is shown to underestimate the loading by a factor of 3 to 12 depending on charge mass; therefore, the impact-and-blast scenario should be adopted as the design case for protective structure roofs. The beam deck ensures repairability and rapid restoration of critical infrastructure facilities.

Keywords: *protective structure, two-layer roof, combined impact and blast loading, contact charge, RHT model, ANSYS Explicit Dynamics.*

Introduction. Introduction. Against the background of an increasingly complex global security environment and the growing frequency of extreme threats, protective technologies for shallow-buried structures have acquired critical importance for military security, wartime civilian sheltering, and the protection of critical infrastructure. Shallow-buried structures offer tactical adaptability and deployment flexibility in countering precision strikes while maintaining operational stability. The surface protective layer converts the kinetic energy of an incoming munition into internal energy and thereby substantially reduces the transmitted shock: a near-instantaneous impact load is transformed into a load with peak values that the structure is able to sustain. Damage to the buried structure itself is thus avoided, as energy concentration is prevented by confining the damage within the protective layer. Improving the protective performance of such roofs remains a long-standing and decisive line of research in protective engineering [1].

For many urban critical infrastructure facilities – transformer substations, pumping stations, water distribution nodes, and district heating plants – shallow embedment is the rational choice: it preserves access for service openings, ventilation, and cooling, while providing the best cost-to-protection ratio in the form of a buried structure with a protective roof and little or no earth cover. In such a configuration, the roof becomes the governing element of the protection system, and its resistance to combined impact and blast action is of fundamental importance.

Literature analysis. Engineering practice offers several established approaches to enhancing the resistance of roofs over shallow-buried structures. Modular shelters based on paired 12-metre containers filled with a concrete–sand composite have demonstrated effective protection against modern weapons; Atlas Survival Shelters (USA) employs standardized combinations of I-beams and steel plates at a 610 mm spacing. The use of polyurethane foam layers enabled Royal HaskoningDHV (Netherlands) to achieve a 50 % reduction in transmitted pressure (from 42 to 21 kPa) under a lateral detonation of a 15 kg TNT charge. Numerical LS-DYNA simulations of a concrete structure incorporating a polyurethane foam interlayer [1] showed that the protective layer dissipates and transforms the blast energy, extends the duration of shock wave action, and reduces the peak load on the roof, with thicker interlayers providing a marked improvement in blast resistance.

Sandwich panels have been studied extensively as blast-resistant elements. It was established in [2] that within a certain loading range monolithic panels outperform sandwich panels with polymer foam cores: owing to the lower transverse stiffness of the components, a higher transverse velocity of the face sheet develops at the early stage of the response, leading to larger deflections and in-plane stresses despite the high energy-absorbing capacity of the core. Under impulsive loading, however, the core undergoes substantial compressive deformation and absorbs a large amount of impact energy, so that at equivalent mass the sandwich configuration provides better blast resistance than its monolithic counterpart; optimization of the core configuration remains one of the key open issues. Aluminum honeycomb cores have been proposed for the protection of reinforced concrete walls [3], as well as stepwise graded honeycomb cores [4], for which experiments and LS-DYNA simulations demonstrated greater attenuation of the transmitted force compared with concrete panels under identical conditions, and superior blast resistance of graded configurations within a certain loading range.

A parallel line of development concerns composite concrete roof systems. In bridge engineering, the adjacent precast beam system is widely used for spans of 10–30 m: precast reinforced concrete beams are placed on the supports side by side in contact with one another, and a cast-in-place composite topping slab 130–200 mm thick is constructed above them; transverse load distribution is provided by shear-keyed joints, the topping slab, and transverse ties [5]. Structurally, such a system behaves as a single orthotropic plate and, for the same material consumption, possesses a higher flexural stiffness in the span direction than an equivalent solid slab (Fig. 1).

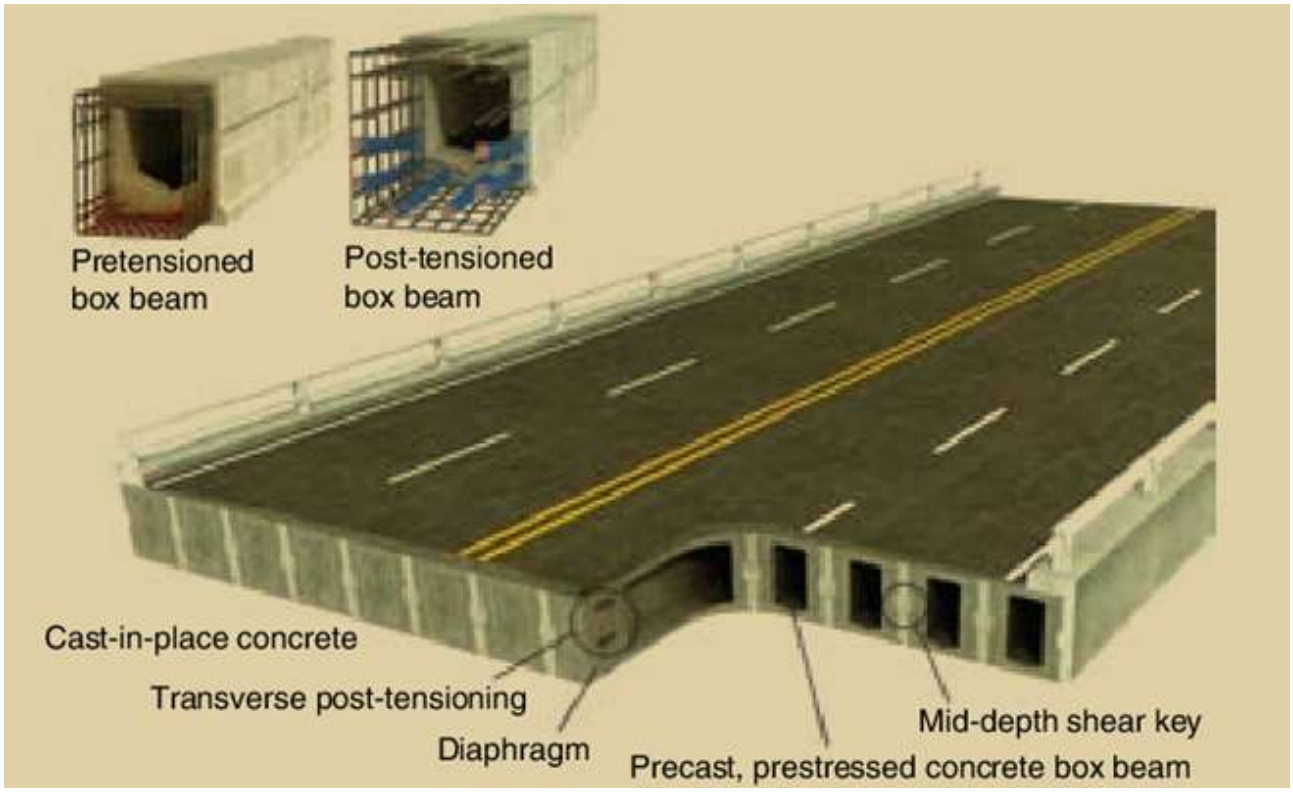


Fig. 1. Structural scheme of a roof composed of adjacent precast beams with a cast-in-place composite topping slab

Fortification practice has long employed spaced (two-layer) roof systems comprising a detonation (sacrificial) burster slab, an air or damping interlayer, and the main load-bearing roof; this concept is embodied in the protective design manuals TM 5-855-1 and UFC 3-340-01 [6, 7]. It has been shown numerically and experimentally [8] that a layered concrete structure with an air gap effectively mitigates the effects of a contact explosion owing to the large mismatch in wave impedance between concrete and air, while double-roof reinforced concrete systems with an energy-absorbing interlayer have confirmed their protective performance in full-scale close-detonation trials [9]. Nevertheless, the combination of a spaced configuration with a load-bearing deck of adjacent beams has received little attention in application to shallow-buried critical infrastructure facilities, particularly for the most dangerous scenario – the impact of a munition followed by delayed detonation.

Formulation of the unresolved part of the problem and the purpose. Statement of the unsolved part of the problem and the objective. The review shows that

spaced (double-layer) protective roofs and adjacent precast beam decks have so far been developed as separate lines of engineering practice: the former in fortification design, the latter in bridge construction. Their combination – a burster slab and an air gap over a load-bearing deck of adjacent beams – has not been investigated for shallow-buried critical infrastructure facilities. Furthermore, the available studies of combined penetration and explosion effects deal mainly with cratering and perforation of massive targets, whereas the stress time histories of a spaced roof under the sequential action of projectile impact and delayed detonation have not been compared with those produced by the simplified contact-charge design scheme; the error introduced by such a simplification therefore remains unquantified.

The aim of this study is to substantiate, by means of numerical simulation, the effectiveness of a two-layer roof for a shallow-buried protective structure – consisting of an upper solid slab (burster layer), an air gap, and a load-bearing deck of adjacent concrete beams – under the impact of a munition followed by its detonation. To this end, the stress-strain state of the roof is analysed in a coupled "impact + detonation" formulation, compared with the response to a surface-laid charge of the same mass, and examined in a parametric series of charge masses from 100 to 500 kg TNT equivalent.

Main part (Results). The simulations were performed in ANSYS Explicit Dynamics using a coupled Euler-Lagrange formulation. The computational model (Fig. 2) comprises a box-type reinforced concrete structure with a two-layer roof: an upper solid slab 600 mm thick, an air gap, and a load-bearing deck of 23 concrete beams with a cross-section of 1200×600 mm; the wall thickness is 1200 mm, and the overall dimensions of the structure are 14,320×12,200×13,750 mm. The structure is surrounded by an air domain with a flow-out boundary condition prescribed on its outer faces to eliminate non-physical wave reflections.

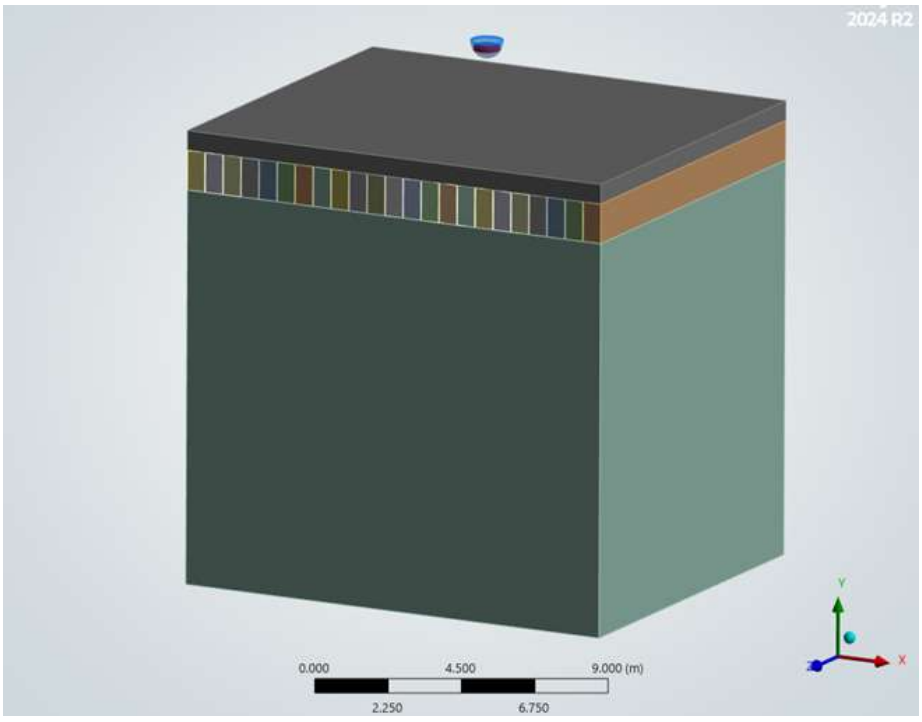


Fig. 2. General view of the computational model:
the structure with a two-layer roof, the air domain, and the munition

The munition is modeled as a moving cylinder containing a 100 kg high-explosive charge in an aluminum casing of 667 kg (total mass 767 kg). The initial velocity of 139 m/s is directed at the upper slab of the roof; detonation is prescribed with a delay of 0.0141 s from the start of the simulation, corresponding to the actuation of a delayed-action fuse after the munition has penetrated into the material of the upper slab – the combined penetration and explosion scenario most dangerous for the structure. The detonation products are described by the JWL equation of state (Table 1), air by the ideal gas equation of state (Table 2), the behavior of concrete by the RHT model (Table 3), and the casing material by an aluminum plasticity model.

The detonation products are described by the JWL (Jones-Wilkins-Lee) equation of state [10]. Library parameters for TNT are used (Table 1); where required, they can be adjusted to match experimentally obtained data:

$$p = A\left(1-\frac{\omega}{R_1 V}\right)e^{-R_1 V} + B\left(1-\frac{\omega}{R_2 V}\right)e^{-R_2 V} + \frac{\omega E}{V}$$

where p is the pressure of the detonation products; V is the relative volume, $V = \rho_0/\rho$, with ρ_0 the initial density of the explosive and ρ the current density; E is the internal energy per unit of current volume ($E = \rho_0 e$), e is the specific internal energy; A, B, R_1, R_2, ω are empirical constants of the particular explosive; ω is the Grüneisen coefficient.

Table 1

Parameters of the JWL equation of state for the explosive (TNT)

Parameter	Symbol	Value	Units
Density	ρ	1630	kg/m^3
Coefficient A	A	$3.7377\cdot10^{11}$	Pa
Coefficient B	B	$3.7471\cdot10^{9}$	Pa
Coefficient R1	R_1	4.15	–
Coefficient R2	R_2	0.9	–
Coefficient ω	ω	0.35	–
Detonation velocity (C–J)	D	6930	m/s
Specific detonation energy (C–J)	E_0	$3.681\cdot10^{6}$	J/kg
Detonation pressure (C–J)	P_{CJ}	$2.1\cdot10^{10}$	Pa

The air domain is described by the ideal gas equation of state; the parameters used are given in Table 2.

Table 2

Parameters of the air model (ideal gas equation of state)

Parameter	Symbol	Value	Units
Density	ρ	1.225	kg/m^3
Specific heat at constant volume	c_v	717.6	J/(kg·°C)
Adiabatic exponent	γ	1.4	–
Reference temperature	T_0	15.05	°C
Specific internal energy	e	$2 \cdot 10^5$	J/kg

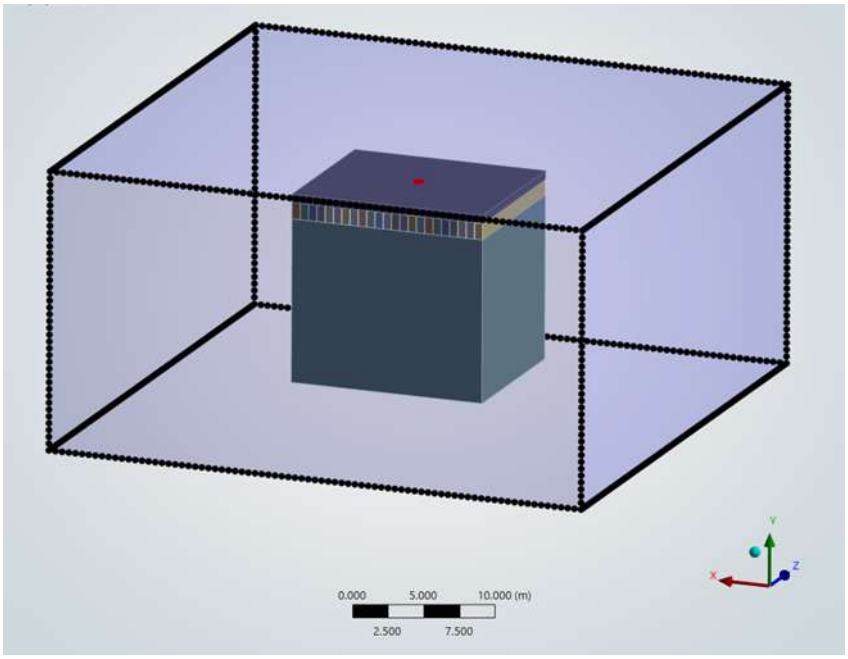


Fig. 3. Eulerian mesh

The behavior of concrete under high-rate loading is described by the RHT (Riedel-Hiermaier-Thoma) model [11], developed at the Fraunhofer Ernst-Mach-Institut specifically for hydrocode simulations of concrete subjected to blast and penetration. The model was calibrated against inverse planar plate impact tests and penetration experiments and has since become one of the standard concrete models in ANSYS Explicit Dynamics for problems of this class. It combines, within a single formulation, the features essential for the present problem: the pressure dependence of strength over the range from tensile spall to high-pressure confinement, the dependence on the third invariant of the stress tensor, the increase of strength with strain rate, porous compaction described by the P–α equation of state, and the accumulation of damage with subsequent softening and transition to the residual strength of the crushed material. This makes it possible to reproduce, in one simulation, both the local crushing of the burster slab in the contact zone and the predominantly elastic wave response of the load-bearing deck.

The numerical values of the parameters for B50 reinforced concrete are given in Table 3.

Table 3

Parameters of the B50 reinforced concrete model (RHT model)

Parameter	Symbol	Value	Units
General properties			
Density	ρ	2786.9	kg/m^3
Specific heat at constant pressure	c_p	654	J/(kg·°C)
P–α equation of state			
Solid material density	ρ_s	2750	kg/m^3
Sound speed in the porous material	c_0	2920	m/s
Initial compaction pressure	P_e	$2.33 \cdot 10^7$	Pa
Solid compaction pressure	P_s	$6 \cdot 10^9$	Pa
Compaction exponent	n	3	–
Polynomial equation of state			
Coefficient A1	A_1	$3.527 \cdot 10^{10}$	Pa
Coefficient A2	A_2	$3.958 \cdot 10^{10}$	Pa
Coefficient A3	A_3	$9.04 \cdot 10^9$	Pa
Coefficient B0	B_0	1.22	–
Coefficient B1	B_1	1.22	–
Coefficient T1	T_1	$3.527 \cdot 10^{10}$	Pa
Coefficient T2	T_2	0	Pa
RHT concrete strength model			
Cap on the elastic surface	–	Yes	–
Compressive strength	f_c	$7.019 \cdot 10^7$	Pa
Tensile strength ratio	f_t/f_c	0.2147	–
Shear strength ratio	f_s/f_c	0.34	–
Intact failure surface constant	A	2.05	–
Intact failure surface exponent	n	0.7	–
Tension/compression meridian ratio	$Q_{2.0}$	0.6805	–
Brittle-to-ductile transition	BQ	0.0105	–
Hardening slope	–	2	–
Elastic strength / *ft*	–	0.7	–
Elastic strength / *fc*	–	0.53	–
Residual (fractured) surface constant	B	1.6	–
Residual (fractured) surface exponent	m	0.61	–
Compressive strain rate exponent	α	0.032	–
Tensile strain rate exponent	δ	0.036	–
Maximum fracture strength ratio	SFMAX	$1 \cdot 10^{20}$	–
Damage constant D1	D_1	0.06	–
Damage constant D2	D_2	1	–
Minimum strain to failure	$\varepsilon_{f\,min}$	0.01	–
Residual shear modulus fraction	–	0.25	–
Shear modulus	G	$1.875 \cdot 10^{10}$	Pa

An adaptive approach was adopted for the Lagrangian mesh of the structure: the element size varies from 0.15 m in the impact zone to 0.5 m away from the detonation point, which made it possible to economize computational resources without loss of accuracy in the critical region; the mesh contains 142,534 nodes and 442,800 elements. The air and the detonation products are discretized with an Eulerian mesh with an element size of 0.5 m (see. Fig. 3). The interaction between the Eulerian and Lagrangian domains is handled by a coupled contact algorithm; the response parameters are recorded by gauges located in the upper slab, in the air gap, and in the deck beams.

Results and discussion. The interaction of the munition with the roof exhibits a clearly staged character. During the first stage, the kinetic impact takes place: the munition strikes the upper slab at 139 m/s, local crushing of concrete develops in the contact zone, and the munition decelerates and embeds itself into the slab material, expending its kinetic energy on penetration.

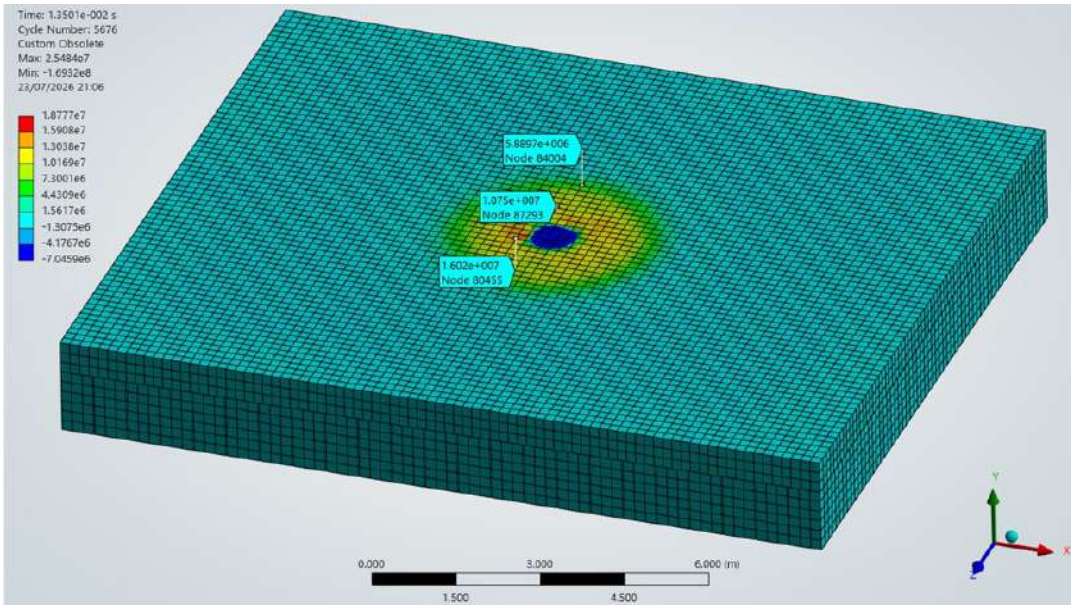
During the second stage, 14.1 ms into the process, the charge detonates. The detonation products expand predominantly into the upper half-space and into the crater formed by the impact; a zone of intense damage develops in the upper slab, localized around the point of detonation. The sequence of stress wave propagation through the structure: the compression wave travels through the upper slab and is partially reflected from its lower free surface (which gives rise to the characteristic spallation confined to the burster layer), so that only a substantially attenuated air-transmitted load reaches the beam deck through the gap.

The air gap plays the key role here. Because of the wave impedance mismatch at the concrete–air interface, direct transmission of the stress wave from the upper slab into the deck is precluded, and what began as a contact–penetration explosion is transformed, as far as the load-bearing layer is concerned, into an air load distributed over the deck area with far lower peak pressure and impulse. The stress fields in the upper slab and in the deck in Figs. 4 (, b): in the upper slab the stresses reach failure levels within a radius of several metres from the detonation point, whereas in the deck beams the stress peaks are concentrated directly beneath the impact zone and at the supports and decay rapidly along the span; the joints between adjacent beams restrict the spread of damage to neighbouring elements, effectively acting as energy dissipators.

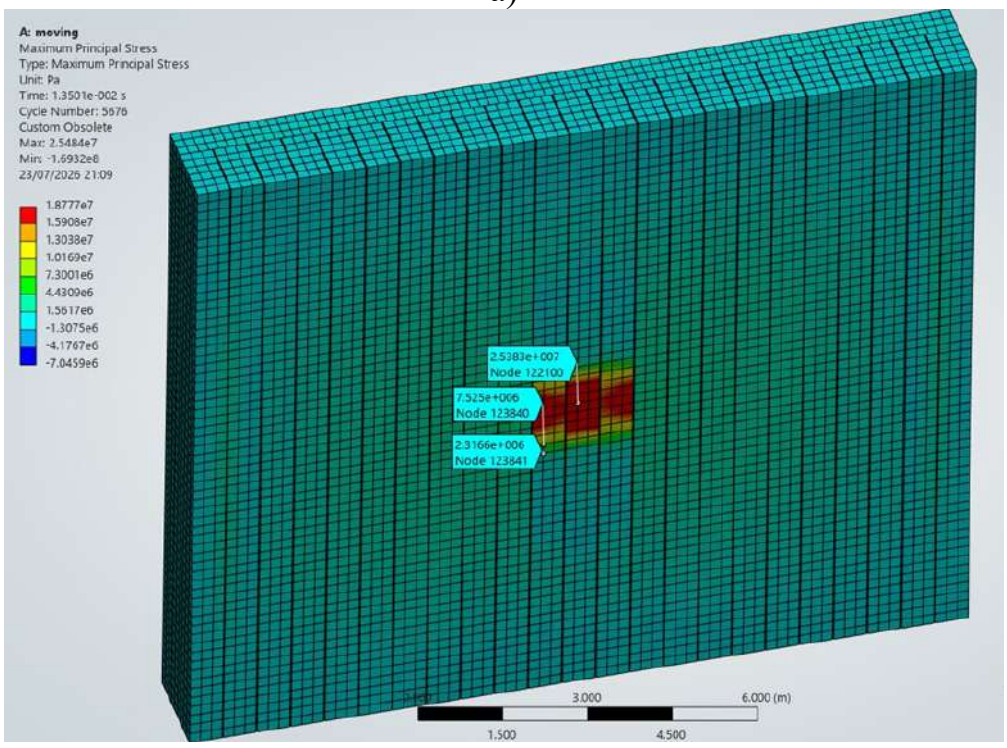
The overall picture of the stress–strain state (Fig. 4) confirms the design intent of the structure: the upper slab performs its function as a burster layer, taking upon itself both the penetration and the detonation, while damage to the load-bearing deck is confined to one to three beams beneath the impact zone and the rest of the deck retains its load-bearing capacity – the recorded peak stresses in the beams do not exceed the dynamic strength of concrete, allowing for the strain-rate strength enhancement captured by the RHT model. A comparison with the design case of contact detonation directly on the load-bearing roof shows a reduction of the transmitted load by an order of magnitude or more, in agreement with the results of [8].

In the detonation zone, the contact pressures reach gigapascals, and the material of the upper slab exceeds its strength limit almost instantaneously. Once the strength limit is reached, the RHT model activates damage accumulation and softening: failed elements shed their stresses. This is why the stress plots show only modest residual stresses in the impact zone of the upper slab – not because the loading is small, but

because the material has already failed and can carry no more. The deck, by contrast, remains largely elastic and therefore exhibits genuinely high elastic peaks.



a)



b)

Fig. 4. Stress-strain state of the deck: a) upper part; b) lower part

On the lower surface of the deck beams, the tensile stresses reach 18.7–25.3 MPa. According to the material card (B50: $f_c = 70$ MPa, $f_t/f_c = 0.2147$), the static tensile strength is approximately 15 MPa, so that without allowance for dynamic strengthening, cracking would have to be expected. At the strain rates typical of blast loading, however, the dynamic tensile strength of concrete increases by a factor of two or more (accounted for in

the RHT model through the exponent δ), so the peak values lie at the strength limit, probably without through-thickness failure – consistent with the fact that the maxima are localized only in the zone beneath the impact. In a real structure, this tension is carried by the bottom flexural reinforcement of the beams, which is absent from the homogenized concrete model; the actual safety margin is therefore higher than the simulation indicates.

At the same time, the lower part of the structure sustains appreciable damage, which may be accompanied by concrete debris falling onto the equipment housed inside; it is advisable to allow for this by providing anti-spall protection (a suspended mesh or lining) beneath the deck.

The question of methodology that deserves separate attention is whether the full "casing impact + detonation" sequence has to be modeled, or whether the simplified design scheme with a contact charge of the same mass is sufficient. To answer it, a comparative simulation of a contact charge acting on the same roof was carried out (Fig. 5); for spaced roofs of critical infrastructure facilities, such a comparison is virtually absent from the literature.

In the penetration–explosion scenario, the casing strikes the slab at t ≈ 13 ms, and σ_1 jumps from about 2.9 to 25.5 MPa – a roughly ninefold increase – while the detonation of the charge at 14.1 ms sustains the high stress level. Thereafter, the stresses oscillate in the range of 18–25 MPa with a slight downward trend as the energy is gradually dissipated through fracture and wave scattering. The contact charge, lacking the kinetic component, produces only about 1.5–2 MPa; in other words, the pre-detonation impact raises the maximum tensile stresses in the structure by roughly an order of magnitude.

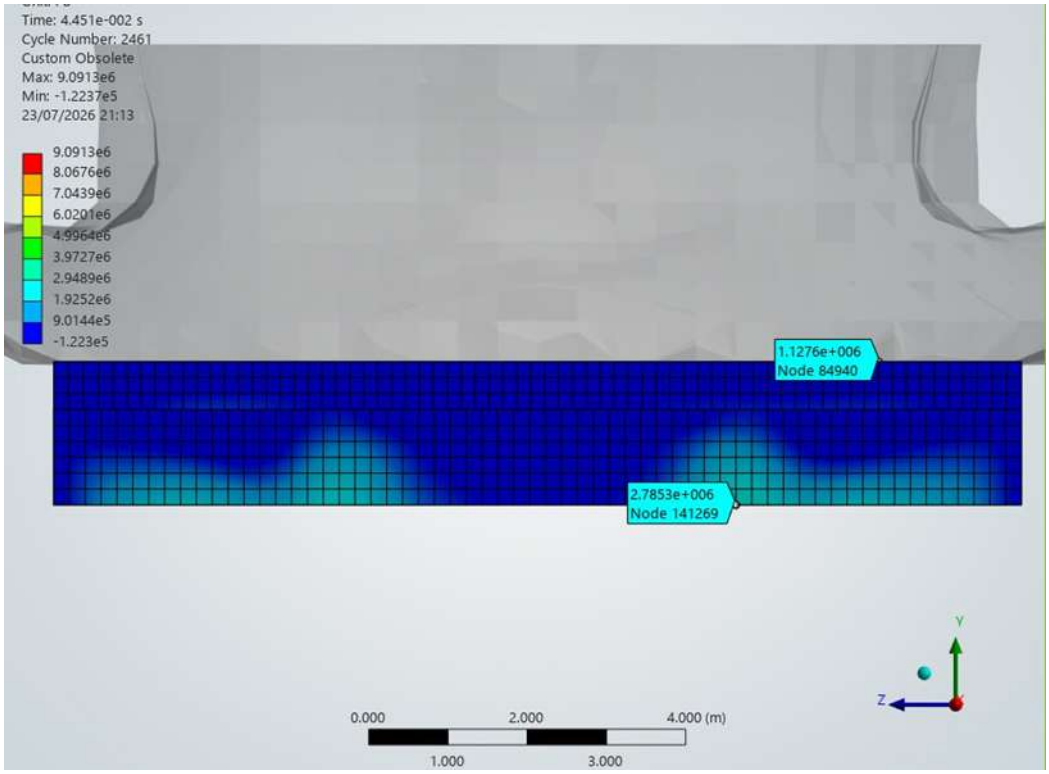


Fig. 5. Maximum principal stresses under a contact charge of the same mass acting on the roof of the structure

The practical implication is that what is critical for the roof of a protective structure is not the contact explosion as such, but the "penetration + detonation" combination – in agreement with the conclusions [12–14] on the amplification of blast damage by prior impact-induced damage.

The maximum tensile stresses develop in the lower part of the structure and amount to $\sigma_1^p = 2.78$ MPa for the contact charge and $\sigma_1^p = 25.48$ MPa for the penetration–explosion loading, giving a ratio $\frac{\sigma_1^p(pen-\exp)}{\sigma_1^p(contact)} \approx 9.2$.

Such a difference is to be expected: a contact charge delivers its energy through an air shock wave, most of which is reflected from the surface, whereas impact followed by detonation in contact establishes a direct mechanical link with the structure. This agrees with [12], where it was shown experimentally and numerically that prior penetration of the projectile substantially amplifies the destructive effect of the explosion – penetration damage weakens the target and facilitates crack initiation and growth; similar conclusions on the mutual amplification of the two factors were reached in [13, 14].

Overall, the results obtained are consistent with the experimental and numerical studies of combined penetration and explosion effects [12–17]; at the same time, the vast majority of those works deal with cratering and perforation of massive targets, whereas a comparison of the stress time histories of a spaced two-layer roof is, to the best of the authors' knowledge, performed here for the first time.

The practical value of damage localization lies in repairability: after an attack, only the upper slab (or a portion of it) and the individual damaged beams need to be replaced rather than the entire roof, which for critical infrastructure facilities translates into rapid restoration of service. A further advantage of the beam deck is its constructability: precast factory-made beams are erected without formwork, and, where required, the deck can be strengthened with a composite topping slab following the proven bridge-engineering scheme [5].

At the next stage, a parametric series of simulations was performed for explosive masses of 100, 200, 300, 400, and 500 kg TNT. The mass of the metal casing in the penetration–explosion scenario remained practically constant (≈ 700 kg), and the impact velocity was kept unchanged (139 m/s). The resulting peak stresses are summarized in Table 4.

Table 4

Peak maximum principal stresses of the parametric series

TNT mass, kg	Contact charge Maximum Principal Stress, MPa	Penetration-explosion Maximum Principal Stress, MPa
100	2.05	25.38
200	3.11	27.05
300	3.26	26.05
400	4.39	26.01
500	9.1	28.09

The results of the parametric series are summarized in Fig. 6, which plots the peak maximum principal stress in the lower part of the structure against the TNT charge mass for both loading scenarios. The two curves behave in strikingly different ways. The contact-charge curve rises steadily from 2.05 MPa at 100 kg to 4.39 MPa at 400 kg, following the power-law trend, and then climbs sharply to 9.1 MPa at 500 kg, marking the change in the load transmission mechanism analyzed below. The penetration-explosion curve, in contrast, remains an almost horizontal line at 25.4–28.1 MPa over the entire mass range. The vertical gap between the two curves – an order of magnitude at the lower masses – narrows toward 500 kg solely because the contact-charge response grows, not because the penetration-explosion loading weakens. The plot thus encapsulates the central finding of the study: the explosive mass governs the structural response only in the contact scenario, whereas the response to a penetrating munition is dictated by its impact velocity.

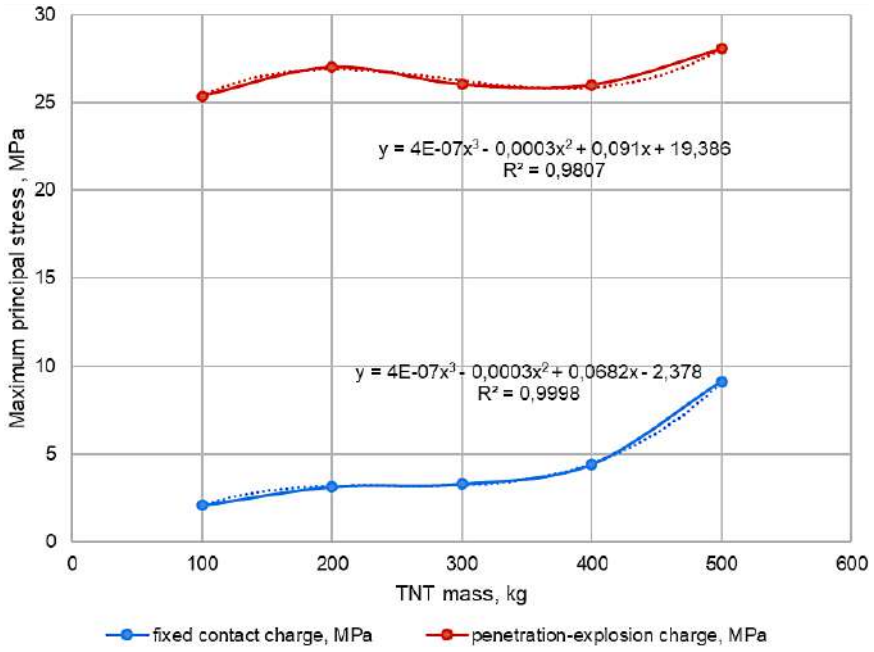


Fig. 6. Maximum principal stress as a function of TNT charge mass for fixed contact charge and penetration–explosion scenarios

For the contact charge, a clear dependence on charge mass is observed. Within the 100–400 kg range, the peak tensile stresses under a contact charge grow according to a power law obtained by regression analysis of the simulation results ($R^2 = 0.93$):

$$\sigma_1^p = 0.20W^{0.51} \approx 0.20\sqrt{W} \qquad 100 \le W \le 400$$

where σ_1^p is the peak maximum principal stress in the lower part of the structure, MPa, and W is the charge mass in TNT equivalent, kg. The exponent of 0.51 falls within the range of 1/3 to 2/3 characteristic of the energy similarity laws of explosion (Hopkinson–Cranz scaling), which supports the physical soundness of the relationship obtained.

At W=500 kg, an abrupt jump to 9.1 MPa is observed against the ~4.7 MPa predicted by extrapolation – an indication of a change in the load transmission mechanism: severe damage to the burster slab, after which the air gap partially loses its screening function.

The penetration–explosion scenario, by contrast, shows no dependence on charge mass. The peak stresses are practically constant at 26.5 ± 1.0 MPa (coefficient of variation 3.6 %) over the entire 100–500 kg range. This directly confirms the mechanism described above: the σ_1 peak is generated by the kinetic impact of the casing, and the contact stress is governed by the impact velocity and the acoustic impedances, both of which are invariant within the series (v = 139 m/s = const; the munition mass of 667.7–785 kg is nearly constant, E_k=*6.4-7.6 MJ*). The explosive mass affects the duration and completeness of the damage, but not the peak tensile stress.

In the acoustic approximation of normal impact between two bodies, the contact stress is determined by the impact velocity and the acoustic impedances of the materials:

$$\sigma_k = v\frac{Z_p Z_c}{Z_p + Z_c},\ Z_p = \rho_p c_p,\ Z_c = \rho_c c_c$$

where v is the impact velocity, m/s; Z_p and Z_c are the acoustic impedances of the casing material and of concrete; and ρ, c are the density and the longitudinal wave velocity, respectively. For the aluminum casing (ρ_p = 2700 kg/m^3, $c_p \approx$ 5300 m/s) and concrete (ρ_c = 2787 kg/m^3, $c_c \approx$ 3600 m/s) at v =139 m/s, this yields $\sigma_k \approx$ 820 MPa.

The peak tensile stresses in the lower part of the structure are related to the contact stress through a transmission coefficient:

$$\sigma_1^p = k_t \sigma_k = k_t v\frac{Z_p Z_c}{Z_p + Z_c},$$

where $k_t \approx 0.03$ is the coefficient of transmission of the compressive contact stress into the tensile stresses in the lower part of the structure, determined from the numerical series (σ_1^p = 26.5 ± 1.0 MPa at $\sigma_k \approx$ 820 MPa) and constant for the given roof geometry. Since none of the quantities entering this relationship depends on the charge mass W, the peak stresses of the penetration–explosion scenario remain practically unchanged throughout the series.

Relation between the two scenarios. The ratio $\frac{\sigma_1^p(pen-\exp)}{\sigma_1^p(contact)}$ decreases monotonically from 12.4 at 100 kg to 3.1 at 500 kg – the contact charge “catches up” only through its own growth, yet even a fivefold increase in explosive mass does not reach the load level produced by the impact of a munition carrying a 100 kg charge. The practical conclusion is that the penetration–explosion scenario must be adopted as the design case for two-layer roofs, its severity being governed by the approach velocity of the munition rather than by the charge mass; substituting an equivalent contact charge underestimates the loading by a factor of 3 to 12, depending on the mass.

Conclusions. Numerical simulation in the coupled Euler-Lagrange formulation of ANSYS Explicit Dynamics has substantiated the effectiveness of a two-layer roof for shallow-buried protective structures of critical infrastructure, composed of an upper solid slab (burster layer), an air gap, and a load-bearing deck of adjacent concrete beams. The simulations show that: 1) the upper slab initiates the detonation of the munition at a distance from the load-bearing layer, converting the most dangerous contact–penetration explosion into a distributed air load on the deck; 2) owing to the wave impedance mismatch at the concrete–air interface, the air gap precludes direct transmission of the stress wave and sharply reduces the transmitted pressure and impulse; 3) damage to the load-bearing deck is confined to one to three beams beneath the impact zone, and the joints between adjacent beams restrict the spread of failure, which ensures the repairability of the structure and rapid restoration of its service.

A quantitative comparison of the scenarios for the baseline case (W = 100 kg) showed that the penetration–explosion loading (casing impact at $t \approx 13$ ms followed by detonation at 14.1 ms) produces peak tensile stresses of σ_1^p=25.48 MPa in the lower part of the structure, against 2.78 MPa for a contact charge of the same mass – roughly nine times higher. The peak values lie at the limit of the dynamic tensile strength of concrete when strain-rate strengthening is taken into account; in a real structure, an additional safety margin is provided by the bottom flexural reinforcement of the beams, which is not represented in the homogenized model.

A parametric series of simulations over the charge mass range of 100–500 kg TNT revealed a fundamentally different character of the two scenarios. For the contact charge, the peak stresses grow according to the power law $\sigma_1^p \approx 0.20 W^{0.51}$ (R^2=0.93), close to proportionality to $\sqrt{W}$ and consistent with the energy similarity laws of explosion; at W=500 kg, a jump to 9.1 MPa was recorded, associated with severe damage to the burster slab and a partial loss of the screening function of the air gap. In the penetration–explosion scenario, by contrast, the peak stresses are practically independent of the charge mass (26.5 ± 1.0 MPa, coefficient of variation 3.6 %) and are governed by the impact velocity and the acoustic impedances of the materials, in accordance with the impedance relationships presented above. The ratio of the peak stresses of the two scenarios decreases from 12.4 at W=100 kg to 3.1 at W=500 kg, yet even a fivefold increase in the mass of the contact charge does not produce a load equivalent to the impact of a munition carrying a 100 kg charge.

It follows that treating penetration and explosive action separately fails to capture the full destructive capability of modern munitions, above all large-caliber weapons with delayed-action fuses employed against buried targets: the simplified contact-charge design scheme underestimates the maximum tensile stresses by a factor of 3 to 12 depending on the charge mass. Protective structures should therefore be assessed in the coupled “impact + detonation” formulation [12–17], with the penetration–explosion scenario adopted as the design case for two-layer roofs – its severity governed by the approach velocity of the munition rather than by the charge mass. Since the relationship $\sigma_1^p = f\left(W\right)$ for the contact charge has been established in this work, further

research should focus on a series of simulations over the impact velocity at $W=const$ to close the generalized relationship $\sigma_1^p = f(W, v)$ and to refine the transmission coefficient k_t for other roof geometries, as well as on optimizing the air gap height, the burster slab thickness, and the beam cross-section for typical threats, and on comparing deck variants with and without a composite topping slab.

References

1. Xu, S., & Liang, Z. (2026). Blast resistance analysis of protective layers for shallow-buried structures. *Journal of Physics: Conference Series*, *3174*, Article 012079. https://doi.org/10.1088/1742-6596/3174/1/012079
2. Langdon, G. S., Karagiozova, D., von Klemperer, C. J., Nurick, G. N., Ozinsky, A., & Pickering, E. G. (2013). The air-blast response of sandwich panels with composite face sheets and polymer foam cores: Experiments and predictions. *International Journal of Impact Engineering*, *54*, 64–82. https://doi.org/10.1016/j.ijimpeng.2012.10.015
3. Yang, R., Guo, Y., Zhang, T., Zhang, R., Wang, K., Song, D., & Zhang, J. (2025). Numerical study on the impact resistance performance of RC walls protected by honeycomb sandwich panels. *Buildings*, *15*(21), Article 3921. https://doi.org/10.3390/buildings15213921
4. Li, S., Li, X., Wang, Z., Wu, G., Lu, G., & Zhao, L. (2016). Finite element analysis of sandwich panels with stepwise graded aluminum honeycomb cores under blast loading. *Composites Part A: Applied Science and Manufacturing*, *80*, 1–12. https://doi.org/10.1016/j.compositesa.2015.09.025
5. National Academies of Sciences, Engineering, and Medicine. (2023). *Guidelines for adjacent precast concrete box beam bridge systems* (NCHRP Research Report 1026). The National Academies Press. https://doi.org/10.17226/27029
6. U.S. Department of the Army. (1986). *Fundamentals of protective design for conventional weapons* (TM 5-855-1). Headquarters, Department of the Army.
7. U.S. Department of Defense. (2002). *Design and analysis of hardened structures to conventional weapons effects* (UFC 3-340-01).
8. Yu, X., Chen, L., Fang, Q., Hou, X., & Fan, Y. (2018). Blast mitigation effect of the layered concrete structure with an air gap: A numerical approach. *International Journal of Protective Structures*, *9*(4), 432–460. https://doi.org/10.1177/2041419618766951
9. Lal, H., Varma, K. R., & Sethi, S. V. (2000). Test evaluation of blast protective double roof RCC structure. In N. Jones & C. A. Brebbia (Eds.), *Structures under shock and impact VI* (WIT Transactions on the Built Environment, Vol. 48, pp. 115–119). WIT Press.
10. Lee, E. L., Hornig, H. C., & Kury, J. W. (1968). *Adiabatic expansion of high explosive detonation products* (Report UCRL-50422). Lawrence Radiation Laboratory, University of California. https://doi.org/10.2172/4783904
11. Riedel, W., Thoma, K., Hiermaier, S., & Schmolinske, E. (1999). Penetration of reinforced concrete by BETA-B-500: Numerical analysis using a new macroscopic concrete model for hydrocodes. In *Proceedings of the 9th International Symposium on Interaction of the Effects of Munitions with Structures* (pp. 315–322).
12. Wei, W.-L., Chen, Y.-Q., Wang, Z.-Q., Li, S.-T., & Hang, C.-L. (2023). Research on damage effect of penetration and explosion integration based on volume filling method. *International Journal of Impact Engineering*, *177*, Article 104591. https://doi.org/10.1016/j.ijimpeng.2023.104591
13. Geng, H., Lu, H., Sun, S., Yue, S., Song, C., & Feng, S. (2020). Experimental study and damage effect analysis of concrete structures under the combined loadings of penetration and explosion. *Shock and Vibration*, *2020*, Article 2137945. https://doi.org/10.1155/2020/2137945
14. Yang, G., Wang, G., Lu, W., Yan, P., & Chen, M. (2018). Combined effects of penetration and explosion on damage characteristics of a mass concrete target. *Journal of Vibroengineering*, *20*(4), 1632–1651. https://doi.org/10.21595/jve.2017.18522
15. Lee, M., Kristoffersen, M., & Børvik, T. (2026). Dynamic response of thin concrete slabs subjected to sequential projectile impact and blast loading: An experimental and numerical investigation. *International Journal of Protective Structures*. Advance online publication. https://doi.org/10.1177/20414196251339824

16. Cheng, Y. H., Zhou, F., Wu, H., & Fang, Q. (2022). Resistance of composite target against combined effects of large caliber projectile penetration and successive charge explosion. *International Journal of Impact Engineering*, *168*, Article 104288. https://doi.org/10.1016/j.ijimpeng.2022.104288
17. Del Linz, P., Fan, S. C., & Lee, C. K. (2016). Modeling of combined impact and blast loading on reinforced concrete slabs. *Latin American Journal of Solids and Structures*, *13*(12), 2266–2282. https://doi.org/10.1590/1679-78252516

АНОТАЦІЯ

Мета. Обґрунтування конструктивного рішення двошарового покриття малозаглиблених захисних споруд критичної інфраструктури та кількісна оцінка його напружено-деформованого стану при ударно-вибуховій дії боєприпасу порівняно з дією накладеного заряду.

Методика. Чисельне моделювання у зв'язаній ейлерово-лагранжевій постановці ANSYS Explicit Dynamics. Бетон описано моделлю міцності RHT з рівнянням стану P–α, продукти детонації – рівнянням стану JWL, повітря – моделлю ідеального газу. Розглянуто покриття у складі верхньої жертовної плити товщиною 600 мм, повітряного прошарку та несучого настилу із суміжних бетонних балок. Боєприпас містить 100 кг вибухової речовини в алюмінієвому корпусі, швидкість підльоту 139 м/с, уповільнення підриву 14,1 мс. Виконано параметричну серію розрахунків для мас заряду 100–500 кг у тротиловому еквіваленті.

Результати. Встановлено, що ударно-вибухове навантаження створює в нижній частині конструкції пікові розтягувальні напруження 25,5 МПа проти 2,78 МПа при накладеному заряді тієї ж маси. Для накладеного заряду отримано степеневу залежність пікових напружень від маси $\sigma_1^p \approx 0.20W^{0.51}$, узгоджену з законами енергетичної подібності вибуху; пік ударно-вибухового сценарію практично не залежить від маси заряду (26,5 ± 1,0 МПа) і визначається швидкістю удару та акустичними імпедансами матеріалів. Пошкодження настилу локалізуються в межах однієї-трьох балок під зоною удару.

Наукова новизна. Вперше виконано порівняння часових історій напружень рознесеного двошарового покриття при дії накладеного заряду та у зв'язаному сценарії «удар + детонація»; запропоновано інженерну залежність пікових розтягувальних напружень через коефіцієнт передачі контактного напруження співударяння.

Практична значимість. Показано, що спрощена розрахункова схема накладеного заряду занижує навантаження у 3–12 разів залежно від маси, тому розрахунковим випадком для покриттів захисних споруд слід приймати ударно-вибуховий сценарій. Балковий настил забезпечує ремонтопридатність і швидке відновлення функціонування споруд критичної інфраструктури.

***Ключові слова*:** *захисна споруда, двошарове покриття, ударно-вибухове навантаження, накладений заряд, модель RHT, ANSYS Explicit Dynamics.*

date of first submission of the article to the publication	07/09/2026
date of acceptance of the article for publication after review	08/10/2026
date of publication	09/30/2026

© 2026. N. Zuievska, V. Berezdetskyi, D. Darmostuk, R. Semchuk, O. Khalymendyk
Published by the Dnipro University of Technology on behalf of Collection of Research Papers of the National Mining University. ISSN 2521-6635 (Online) | ISSN 2071-1859 (Print). This is an Open Access article distributed under the terms of the Creative Commons Attribution License (http://creativecommons.org/licenses/by/4.0/), which permits unrestricted reuse, distribution, and reproduction in any medium, provided the original work is properly cited.